Test-bench for the experimental characterization of porous material used in thermoacoustic refrigerators

Gaelle Poignand, Come Olivier and Guillaume Penelet

Citation: The Journal of the Acoustical Society of America **152**, 2804 (2022); doi: 10.1121/10.0015051
View online: https://doi.org/10.1121/10.0015051
View Table of Contents: https://asa.scitation.org/toc/jas/152/5
Published by the Acoustical Society of America

JASA ARTICLE

Test-bench for the experimental characterization of porous material used in thermoacoustic refrigerators

Gaelle Poignand,[a] Come Olivier,[b] and Guillaume Penelet
Laboratoire d'Acoustique de l'Université du Mans (LAUM), UMR 6613, Institut d'Acoustique–Graduate School (IA–GS), CNRS, Le Mans Université, Le Mans, France

ABSTRACT:
The design of thermoacoustic coolers involves an adequate modeling of the thermoacoustic core's performance, which requires, in particular, a precise knowledge of their thermo-physical properties. Materials such as wire mesh stacks, foams, or compressed fibrous media are hard to describe, and their thermo-physical properties are rarely well enough quantified. Moreover, the classical linear thermoacoustic theory is not sufficient to accurately describe the performance of these materials. This paper deals with the experimental performance characterization of various materials for thermoacoustic heat pumping. A dedicated experimental test-bench has been specially developed, which is composed of two loudspeakers placed at opposite ends of a waveguide containing the porous material and a feedback loop to control the acoustic field in the porous material. Its originality is attributable to the possibility of identifying the optimal acoustic field, specific to each material, that maximizes the temperature difference at the ends of the material. Moreover, a specific protocol is implemented to access and compare the thermoacoustic heat flux through various materials at these optimal acoustic fields. Comparison of the experimental and theoretical results shows a reasonable agreement. © *2022 Acoustical Society of America*. https://doi.org/10.1121/10.0015051

(Received 8 July 2022; revised 20 September 2022; accepted 14 October 2022; published online 8 November 2022)
[Editor: Philippe Blanc-Benon] Pages: 2804–2815

I. INTRODUCTION

Thermoacoustic refrigerators[1] are thermal machines that exploit the interaction between an acoustic oscillation and a porous material. Such an interaction leads to the generation of a heat flux along the porous material, which enables the transport of heat from a cold to a hot reservoir. Thermoacoustic refrigerators are usually composed of an acoustic source coupled to a resonator in which is inserted the thermoacoustic core, consisting of an open cell porous material equipped with heat exchangers on each side. These machines are characterized in particular by their simple construction (the only moving mechanical component being the acoustic source) and their low environmental impact, as they operate with noble gases or their mixture.[2]

Since the pioneering works of Merkli and Thomann,[3] who first observed the thermoacoustic cooling effect, various prototypes of thermoacoustic coolers[4] have been developed with different architectures. Among others, one can mention the beer cooler, which is a heat-driven refrigerator,[1] the traveling-wave thermoacoustic refrigerator for ice cream storage,[5] the coaxial thermoacoustic-Stirling cooler,[6] the compact coaxial refrigerator,[7,8] or the multi-stage thermoacoustic-Stirling cooler.[9] These machines can be categorized into standing-wave or traveling-wave devices based on the characteristics of the acoustic field inside the porous material, which is called a stack in the standing-wave machines or a regenerator in the traveling-wave ones. Gas parcels in a regenerator follow an inherently reversible thermodynamic cycle, and the associated thermoacoustic process is expected to be more efficient than the one occurring in a stack. For the travelling-wave devices, a near isothermal condition is required in the regenerator. This condition is satisfied if the size of the material's pore is much smaller than the thermal penetration depth to ensure a very good heat contact between the gas and the solid material. Because of this constraint, regular straight-pore regenerators are rarely mentioned in the literature, and stacked-screen regenerators are mostly preferred. However, the linear thermoacoustic theory[10] widely used to design and predict the performance of thermoacoustic devices is based on regular straight pores. Swift and Ward[11] have gone beyond this theory by proposing an empirical description of stacked-screen regenerators, and the experimental studies of Ueda *et al.*[12] and of Hsu and Biwa[13,14] have allowed advances in the theoretical description of such regenerators. Nevertheless, other materials with irregular pore geometries can also be employed. Experimental performance of some materials used as regenerators has been studied by Abduljalil *et al.*[15] in the case of a thermoacoustic engine. However, there is a lack of experimental data characterizing the performance of materials employed in thermoacoustic refrigerators.

The goal of this study is to experimentally investigate various porous materials for thermoacoustic refrigeration. For this purpose, a dedicated test-bench is developed to characterize experimentally the performances of these

[a]Electronic mail: gaelle.poignand@univ-lemans.fr
[b]Also at: Centre de Transfert de Technologie du Mans (CTTM), Le Mans, France.

https://doi.org/10.1121/10.0015051

materials. It is composed of two loudspeakers set at the opposite ends of a waveguide in which a porous material is introduced. An acoustic feedback loop links the back cavity of one of the loudspeakers to the opposite side of the waveguide to control the acoustic field inside the material (in terms of acoustic pressure, acoustic velocity, and phase between them). The originality of this test-bench lies in the fact that in addition to access to thermo-physical properties of the material (such as its thermal conductivity, porosity, or effective radius), it also allows determination of the optimal acoustic field, specific to each material, which maximizes the temperature difference between its two ends by acting on the voltages supplied to the loudspeakers. The interest of measuring this field is that its theoretical estimation is a hard task since it relies on a complete energy balance of the thermoacoustic core, which requires knowledge of the heat transfer coefficient of the materials considered. In addition, a new protocol is developed to measure the thermoacoustic heat flow along the material. This protocol gives access to a new quantity to estimate the material's efficiency. Materials investigated range from ceramic stacks with square pores, which are usually well described by the linear thermoacoustics theory (and will therefore serve as our validation case), to less simple materials, such as stacked stainless steel mesh grids, which are commonly employed in thermoacoustic devices, to various foams about which little is known[11,13] (such as stainless steel, copper or carbon foams, or compacted glass wool). In Sec. II, theoretical background concerning the thermoacoustic heat flux is given. Then, in Sec. III, the experimental test-bench and the protocol employed to characterize the materials are presented. Section IV discusses the results obtained in terms of optimal acoustic field, temperature difference, and thermoacoustic heat flux along the various materials characterized.

II. THEORETICAL BACKGROUND

We consider a porous material of length L with a porosity ϕ and an effective radius r_0 placed in a waveguide in the presence of a harmonic plane wave propagating along the x axis at an angular frequency ω (see Fig. 1, top right). The interaction between the acoustic wave and the material leads to the generation of a thermoacoustic heat flux Q_{th} along the x axis. In the classical theory of thermoacoustics,[10] this heat flux is defined by the hydrodynamic transport of entropy s carried by the oscillatory axial velocity v_x and averaged over the cross section area A of the channel,

$$Q_{\text{th}} = \frac{1}{2}\rho_m T_m \int \Re\left[s v_x^*\right] dA, \tag{1}$$

where the asterisk * denotes the conjugate of a complex number, and ρ_m and T_m represent the mean density and temperature of the fluid, respectively.

The entropy oscillations s can be expressed as a function of the acoustic pressure p and temperature fluctuation τ, such that

$$s = -\frac{\beta}{\rho_m} p + \frac{c_p}{T_m}\tau, \tag{2}$$

with β the isobaric coefficient of thermal expansion of the fluid and c_p its isobaric heat capacity per unit mass.

For an ideal gas and considering the case of a channel with regular pores, an expression for the temperature oscillation τ can be found from the linear theory[10] that expresses the thermoacoustic heat flux (1) as a function of acoustic pressure and velocity,

$$Q_{\text{th}} = -\frac{1}{2}A\Re\left[g p \langle v_x\rangle^*\right] + \frac{A}{2}\frac{\rho_m c_p}{\omega}\Im\left[g_D\right]\frac{dT_m}{dx}\left|\langle v_x\rangle\right|^2, \tag{3}$$

with $g = (f_\kappa - f_\nu^*)/(1+\sigma)(1-f_\nu^*)$ and $g_D = (f_\kappa + \sigma f_\nu^*)/[(1-\sigma^2)|1-f_\nu^*|^2]$, where σ is the Prandtl number of the gas.

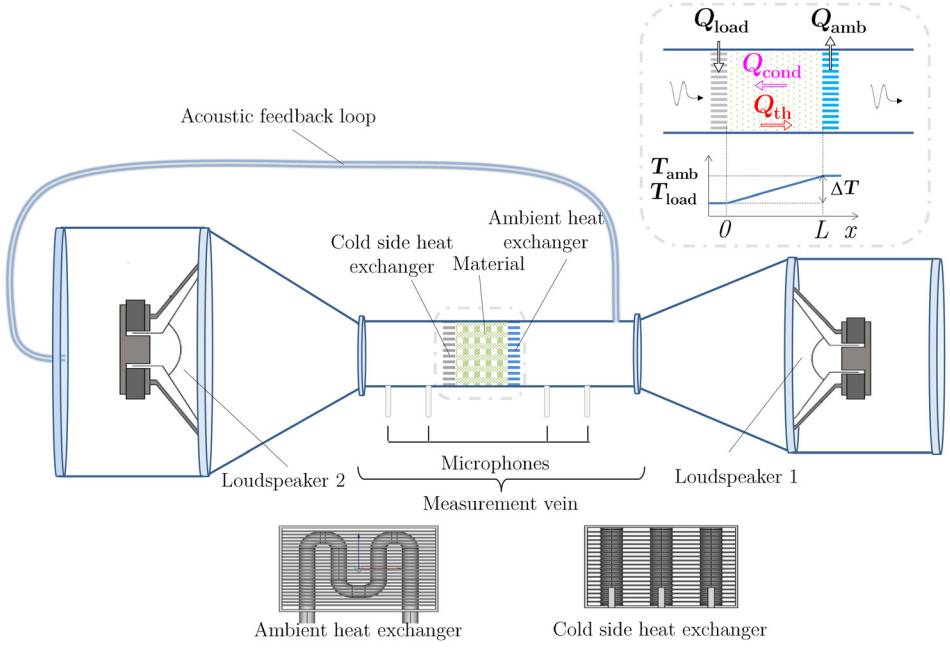

FIG. 1. (Color online) Top right, detailed view of the thermoacoustic core and heat flux involved in the thermoacoustic process. Middle, schematic diagram of the experimental test-bench. Bottom, schematics of the two heat exchangers.

$\Re$, $\Im$ show, respectively, the real part and the imaginary part of a complex quantity, and $\langle\cdots\rangle = (1/A)\int\cdots dA$, the cross-sectional average. f_κ and f_ν are complex Rott functions associated, respectively, with the thermal diffusivity κ and the kinematic viscosity ν of the gas. In the case of circular pores of radius r_0, these functions are written as

$$f_{n=\kappa,\nu} = \frac{2J_1\left[(i-1)\frac{r_0}{\delta_n}\right]}{(i-1)\frac{r_0}{\delta_n}J_0[(i-1)r_0/\delta_n]}, \tag{4}$$

with J_1 and J_0, respectively, the first-order and zeroth-order Bessel function of the first kind, $i^2 = -1$, and $\delta_{n=\kappa,\nu} = \sqrt{2n/\omega}$, the thermal and viscous boundary layer thicknesses.

The expression (3) of the thermoacoustic heat flux is only valid for materials with regular pores,[1] such as arrays of circular, rectangular, and square cross section tubes or an array of pins.[16] For more complex flow channels, theoretical analysis of the oscillatory flow in the material remains an arduous task. Swift and Ward[11] proposed a theoretical model of stacked mesh screen material based on the simple harmonic analysis of the momentum, continuity, and energy equations, where viscothermal effects are described through friction factor, and the heat transfer coefficient is determined via steady-flow data of Kays and London,[17] which depend on the acoustic velocity. Their expression of the heat flux Q_{th} is written as

$$Q_{\text{th}} = \frac{1}{2}A\rho_m T_m \Re\left[\langle s\rangle\langle v_x\rangle^*\right], \tag{5}$$

where the cross-sectional average of entropy and temperature fluctuations are, respectively, given by

$$\langle s\rangle = -\frac{\beta}{\rho_m}p + \frac{c_p}{T_m}\langle\tau\rangle_S \tag{6}$$

and

$$\langle\tau\rangle_S \equiv \frac{\langle\tau v_x\rangle}{\langle v_x\rangle} = \frac{\beta T_m}{\rho_m c_p}\Gamma p - \frac{1}{i\omega}\frac{dT_m}{dx}G\langle v_x\rangle, \tag{7}$$

using

$$\Gamma = \frac{\epsilon_s + \epsilon_h(g_c + e^{2i\theta_p}g_v)}{1 + \epsilon_s + \epsilon_h(g_c + e^{2i\theta_T}g_v)},$$

$$G = \frac{\epsilon_s + \epsilon_h(g_c - g_v)}{1 + \epsilon_s + \epsilon_h(g_c + e^{2i\theta_T}g_v)},$$

$$\epsilon_s = \frac{\phi\rho_m c_p}{(1-\phi)\rho_s c_s}, \quad \theta_p = \text{phase}(\langle v_x\rangle) - \text{phase}(p),$$

$$\epsilon_h = \frac{8ir_0^2}{b(\phi)\sigma^{1/3}\delta_\kappa^2}, \quad \theta_T = \text{phase}(\langle v_x\rangle) - \text{phase}(\langle\tau\rangle_s),$$

$$g_c = \frac{2}{\pi}\int_0^{\pi/2}\frac{dz}{1 + Re_h^{3/5}\cos^{3/5}(z)},$$

$$g_v = -\frac{2}{\pi}\int_0^{\pi/2}\frac{\cos(2z)dz}{1 + Re_h^{3/5}\cos^{3/5}(z)},$$

$$b(\phi) = 3.81 - 11.29\phi + 9.47\phi^2, \quad Re_h = 2|\langle v_x\rangle|\frac{r_0}{\nu},$$

where ρ_s and c_s denote the density and the heat capacity of the solid.

By substituting relations (6) and (7) into expression (5), the thermoacoustic heat flux can be expressed as

$$Q_{\text{th}} = -\frac{1}{2}A\Re\left[(1 - T_m\beta\Gamma)p\langle v_x\rangle^*\right] - \frac{A}{2}\frac{\rho_m c_p}{\omega}\Im[G]\frac{dT_m}{dx}|\langle v_x\rangle|^2. \tag{8}$$

A. Discussion

The thermoacoustic heat flux (3) and (8) are written as the sum of two terms for both cases of the classical thermoacoustic theory for regular pores and the model proposed by Swift and Ward. The first term represents the heat flux Q_{A} caused by the acoustic oscillations, which do not depend on the local temperature gradient. The second term Q_{D} represents the acoustically induced heat flux, which is proportional to the local temperature gradient {and the term $(\rho_m c_p/\omega)\Im[G]|\langle v_x\rangle|^2$ represents an acoustically induced thermal conductivity that acts in addition to the thermal conductivity of the porous material}.

The heat flux Q_{th} has been experimentally characterized by Hsu and Biwa[14] for ceramic materials and stacked-screen regenerators for an engine mode. In their experimental configurations, Q_{th} can be approximated by Q_{D} ($Q_{\text{A}}/Q_{\text{D}} < 0.1$), the temperature difference being fixed at 250 K, and the specific acoustic impedance, defined by the ratio between p and $\langle v_x\rangle$, is tuned to have a magnitude of about $0.3\rho_m c_0$ and a phase of 0°. One of the original aspects of this present paper is the measurement of the heat flux in the case of a refrigerator mode. In that case, the approximation $Q_{\text{th}} \simeq Q_{\text{D}}$ is no more valid. In fact, the heat flux Q_{D} (which depends on the temperature gradient) is always directed from the hot to the cold end of the material: it is opposite in sign compared to the first term Q_{A} and therefore decreases the global heat flux.

Another original aspect of this paper is the experimental investigation of the optimal acoustic field that maximizes the performance of the material. Indeed, there is an optimal acoustic field in terms of acoustic volume flow rate $U = A|\langle v_x\rangle|e^{-i\varphi_{p/U}}$ and relative phase $\varphi_{p/U}$ between the acoustic pressure p and U that maximizes the temperature difference and the thermoacoustic heat flux.[18] An analytic expression of this optimal acoustic field can be obtained by considering that the thermoacoustic heat flux is balanced by the thermal heat conduction through the material. The heat balance is given by (assuming $\Delta T/L \simeq dT_m/dx$)

$$Q_{\text{th}} + Q_{\text{cond}} = 0, \quad \text{with} \quad Q_{\text{cond}} = -k_s(1-\phi)A\frac{\Delta T}{L}, \tag{9}$$

which leads to

$$\frac{\Delta T}{L} = \frac{\frac{1}{2}p|U|\Re\left[ge^{i\varphi}\right]}{\frac{1}{2}\frac{\rho_m c_p}{A\omega}\Im[g_D]|U|^2 + k_s(1-\phi)A}. \tag{10}$$

https://doi.org/10.1121/10.0015051

The temperature difference ΔT and the heat flux Q_{th} reach maximum for

$$|U|_{\text{opt}} = A\sqrt{\frac{2k_s(1-\phi)\omega}{\rho_m c_p \Im[g_D]}}, \tag{11}$$

$$(\varphi_{p/U})_{\text{opt}} = \arctan\left(-\frac{\Im[g]}{\Re[g]}\right), \tag{12}$$

with k_s the thermal conductivity of the material and the acoustic volume flow rate $U = A|\langle v_x\rangle|e^{-i\varphi_{p/U}}$.

The expression of the optimal velocity comes from a balance between the leading flow Q_A proportional to $\langle v_x\rangle$ and the two restrictive fluxes, namely Q_D (proportional to $\langle v_x\rangle^2$) and Q_{cond} (due to the thermal heat conduction through the material). The optimal phase depends only on the function g, which itself depends on the ratios $r_0/\delta_{n=\kappa,\nu}$. For a regenerator $r_0/\delta_{n=\kappa,\nu} \ll 1$, the functions $f_{n=\kappa,\nu}$ have their imaginary part tending to 0, so that $\Im[g] \sim 0$, and hence, as expected, for a regenerator, the optimal phase is almost null. For a stack, $r_0 \sim \delta_{n=\kappa,\nu}$, $\Im[g]$ is not negligible compared to $\Re[g]$, which leads to an optimal phase that deviates from 0.

In our experiments, the heat balance to obtain the temperature field is expected to be more complicated than the one given by the relation (9), especially because of the expected lateral losses through the wall of the waveguide. A global heat balance is necessary to determine the temperature distribution that is coupled to the acoustic field via the thermoacoustic heat flux. The expression (11) of the optimal acoustic field is based on simplified assumptions, which is why, in the following, we have chosen to determine it at the fixed frequency of 100 Hz. The thermoacoustic heat flux is then evaluated through different materials at these optimal acoustic fields and compared to the theoretical expression (3) for ceramic materials considering circular pores, whereas the expression (8) is used for the other materials.

III. EXPERIMENTAL SETUP

An experimental test-bench has been specially designed to evaluate the performance of various porous materials when submitted to a controlled acoustic field of variable pressure amplitude up to 2000 Pa. A schematic view of the test-bench, whose architecture is based on the coaxial refrigerator setup,[19] is given in Fig. 1. The setup is composed of a measurement vein in which a rectangular sample of the porous material under test is inserted between two heat exchangers. On either side of the measurement vein is an acoustic source loaded by a rear cavity. An acoustic feedback loop connects the rear cavity of one of the loudspeakers to the opposite side of the waveguide. This acoustic source, namely, loudspeaker 2 in Fig. 1, behaves mainly as a flow rate source, whereas the other one, namely, loudspeaker 1, can be considered as a pressure source. An early precursor to this approach of independent control of pressure, volume flow, and their relative phase was introduced in a small cubical cavity that contained a stack and four loudspeakers.[18] The two loudspeakers that were aligned along the axis of the pores were driven out-of-phase to control the volume flow of gas through the stack. The second orthogonal pair were driven independently in-phase to control the amplitude of the acoustic pressure. This control of the acoustic field in the present apparatus is performed by adjusting the voltages (in amplitude and phase) supplied to the two acoustic sources. It should be mentioned that the test-bench has been designed to explore a wide range of impedance (in amplitude and phase) at the center of the materials under test to access the optimal acoustic field specific to each material that maximizes the temperature difference.

Two loudspeakers from B&C Speakers (Florence, Italy) (catalog nos. 8BG51 and 10NW64) have been chosen, respectively, as the pressure source and as the flow rate source. The rear cavity volumes of these two sources are, respectively, 9.4 and 14.6 L, and the feedback loop is a flexible tube with a diameter of 2 cm and a length of 1.83 m. A 14.5 cm long cone in series with a 5 cm long rectangular-to-circular adapter connects the front side of each acoustic source to the measurement vein.

The measurement vein is made of PMMA and has a rectangular section of $4 \times 6\,\text{cm}^2$. The heat exchangers are 3D-printed in stainless steel. They each consist of a stack of 2.5 cm long plates of thickness 0.5 mm, separated by 1.5 mm for the cold heat exchanger and 1 mm for the ambient one, as illustrated in Fig. 1 (bottom). The ambient heat exchanger is water-cooled to be kept at room temperature $T_{\text{amb}} \approx 293$ K, whereas the cold heat exchanger is heated by three $\frac{1}{4}$ in. heating cartridges [Omega (Norwalk, CT) HDC00001 high density cartridge heater, $20\,\text{W}\cdot\text{cm}^{-2}$]. The system is filled with air at atmospheric pressure. For all measurements, the frequency is fixed at 100 Hz.

The test-bench is instrumented with two type-K thermocouples to monitor the temperature T_{amb} and T_{load} on either side of the porous material. They are placed on the central axis to determine the axial temperature difference $\Delta T = T_{\text{amb}} - T_{\text{load}}$ across the porous material. They are plugged into a thermocouple data logger (PICO TC-08). The voltages supplied to the speakers are provided by a two-channel function generator (Tektronix AFG3022C) via power amplifiers (QSC RMX 850a). Two pairs of $\frac{1}{4}$ in. microphones [from Bruel & Kjaer (Naerum, Denmark), type 4938 with NEXUS amplifier 2690] are mounted flush to the surface on each side of the porous material. They allow the measurement of the acoustic pressure and the volume velocity on both sides of the material using the two-sensor method. The pair of microphones on the pressure-source side are separated by 4.5 cm, while the other pair are separated by 8.2 cm. Attention has been paid to the relative calibration (both in amplitude and phase) of the microphones realized using a small cavity coupler and to their spacing to minimize measurement errors. A large

variety of porous materials are studied with this test-bench: two square pore ceramic honeycomb catalysts [with 400 and 800 cells per square inch (CPSI)], two metal foams (nickel chrome alloy and copper) and a reticulated vitreous carbon (RVC) foam, a fibrous material (rigid high density glass wool), and randomly stacked stainless steel wire mesh screens. Photographs of all samples are provided in Fig. 2. The geometrical parameters of the materials, their effective radius r_0, and their porosity ϕ are estimated experimentally using the two-source method,[20] which takes advantage of two pairs of microphones on both sides of the material. This method consists in imposing two different acoustic states inside the material (by alternately switching on each loudspeaker, the other being switched off) to access the transfer matrix of the material. One of this matrix's components being the flow resistance, r_0 and ϕ are then estimated by adjusting the experimental and theoretical value of the flow resistance over a large frequency band.

The objective in the following is to experimentally characterize the performance of the materials in terms of optimal acoustic field, temperature difference ΔT, and thermoacoustic heat flux Q_{th}. The different steps of the protocol implemented for each material are described hereafter. Care was taken to wait for temperature stabilization in the entire test-bench before each measurement. The time required for equilibration ranges from a few minutes to 45 min, depending upon the heat capacity of the sample being tested.

- Thermal equilibrium is first achieved without acoustic oscillation, where temperature difference $\Delta T_{\text{No,Ac}}$ across the material is measured for different thermal loads $Q_{\text{load,NoAc}}$ imposed at one side of the material, whereas the other side is maintained at room temperature. The heat balance, presented in Fig. 3(a), deduces the thermal conductivity of the material and the thermal losses Q_{loss} at a given temperature difference.

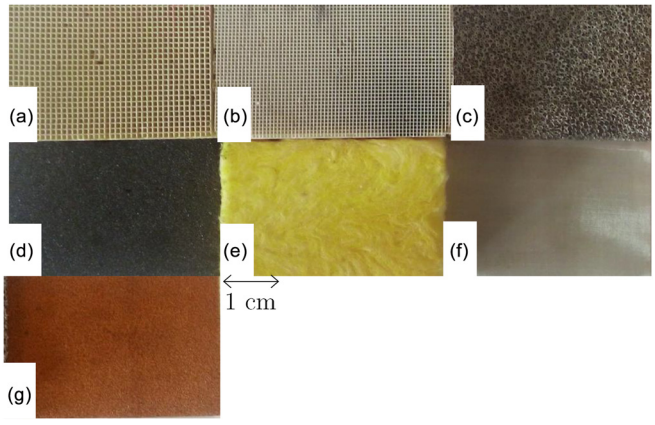

FIG. 2. (Color online) Picture of the different materials studied: (a) 400 CPSI ceramic, (b) 800 CPSI ceramic, (c) nickel-chromium foam, (d) RVC foam, (e) rigid high density glass wool, (f) stainless steel 304L wire mesh, and (g) copper foam.

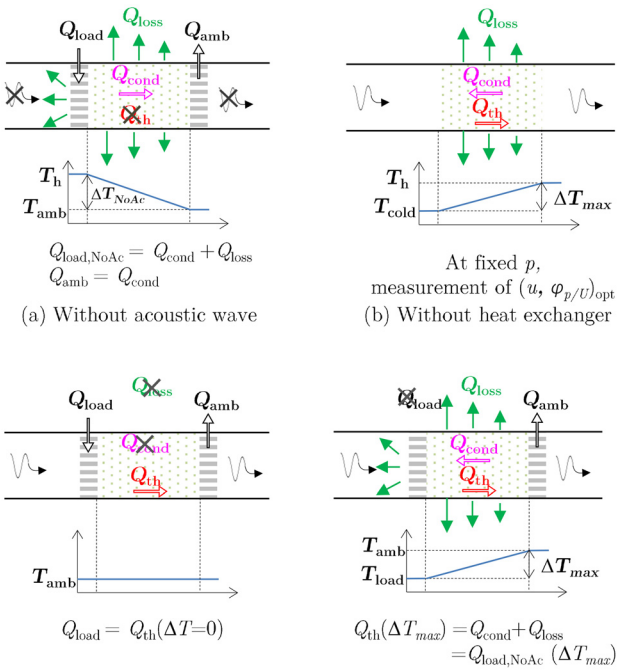

FIG. 3. (Color online) Schematic diagrams of the heat flux involved in the thermoacoustic process for different configurations: without acoustic oscillation (a), with acoustic oscillation without heat exchanger (b), with acoustic oscillation when the thermal load Q_{load} is increased until ΔT is zero (c), and with acoustic oscillation but without thermal load (d).

- The optimal acoustic field maximizing the temperature difference ΔT is sought for different acoustic pressures. Since the thermal inertia of the heat exchangers increases significantly the time for stabilization of the temperatures, these measurements are made with the two heat exchangers removed from the measurement vein [see Fig. 3(b)]. The optimal acoustic field for the temperature difference is considered identical with or without the heat exchangers.
- At the optimal acoustic field previously determined, the temperature difference ΔT is measured for several thermal loads Q_{load} imposed at the cold side heat exchanger. The temperature difference ΔT decreases with increasing thermal loads Q_{load} until it cancels and then changes sign. When the temperature difference is null, as illustrated Fig. 3(c), there is no heat conduction through the material nor heat losses, and, therefore, the thermoacoustic heat flux $Q_{\text{th}}(\Delta T = 0)$ is exactly balanced by the thermal heat load Q_{load}. The value for which Q_{load} cancels the temperature difference ΔT provides directly the first term Q_{A} of the heat flux Q_{th}, i.e., the thermoacoustic heat flux Q_{th} without the temperature difference ΔT (the heat flux Q_{D} being null).
- A global heat balance is needed to access the total thermoacoustic heat flux with a non-zero temperature gradient, the second term Q_{D} depending on the temperature. In the experimental part, we present the minimum value of the thermoacoustic heat flux Q_{th}, which is reached

https://doi.org/10.1121/10.0015051

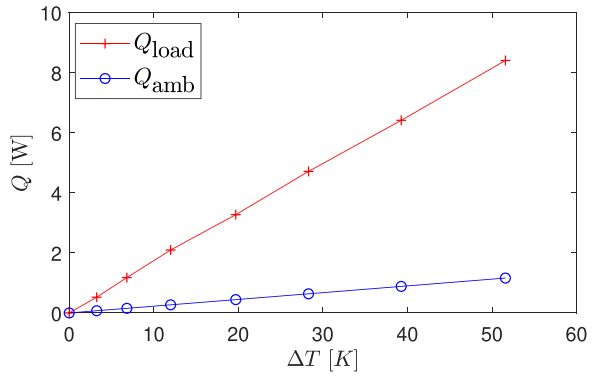

FIG. 4. (Color online) Thermal power Q_{load} imposed at one side of the material and heat Q_{amb} extracted at the other side as functions of the temperature difference ΔT measured across the 400 CPSI ceramic material without acoustic wave.

when there is no thermal load $Q_{load} = 0$, i.e., when the temperature difference ΔT and hence the flux Q_D are maximum. In this particular case [see Fig. 3(d)], the thermoacoustic heat flux $Q_{th}(\Delta T_{max})$ is balanced by the heat conduction Q_{cond} through the material and the thermal losses Q_{loss}. An estimation of $Q_{th}(\Delta T_{max})$ is then given by considering that the sum $Q_{cond} + Q_{loss}$ is equivalent to the thermal heat load $Q_{load,NoAc}$ needed to impose this temperature difference ΔT_{max} without acoustic oscillation (previously measured in step 1) so that $Q_{th}(\Delta T_{max}) = Q_{load,NoAc}(\Delta T_{max})$.

The protocol thus defined allows us to access the minimum and maximum value of the thermoacoustic heat flux noted, respectively, as $Q_{th}(\Delta T_{max})$ and $Q_{th}(\Delta T = 0) = Q_A$. In Sec. IV, the experimental results are presented for each step of the protocol.

IV. EXPERIMENTAL RESULTS

A. Thermal measurement without acoustic oscillation

When no acoustic oscillations are present, the thermal conductivity k_s of the porous materials is evaluated in steady-state regime by measuring the temperature difference ΔT across the material when a known heat load $Q_{load,NoAc}$ is imposed at one side of the material, and the temperature returns to room temperature at the other side. The thermal power Q_{load} is given by the electrical power input supplied to the cartridges. The heat flux Q_{amb} extracted by water circulating in the ambient heat exchanger is evaluated via the formula $Q_{amb} = U_w c_w \Delta T_w$ by measuring the (small) temperature increase ΔT_w between the intake and the outlet of the exchanger and with the specific heat capacity $c_w = 4.1796$ kJ·kg^{-1}·K^{-1}. The mass flow rate U_w of water circulating through the exchanger is deduced from the weight of the flow collected during 2 min.

At thermal equilibrium, the temperature difference ΔT established across the material through thermal conduction is such that

$$Q_{cond} = -k_s(1-\phi)A\frac{\Delta T}{L}, \tag{13}$$

the heat transfer by conduction in the air, is considered negligible in comparison with the one through the solid walls. The heat balance at the ambient heat exchanger [see Fig. 3(a)] reveals that the heat Q_{amb} removed from the ambient heat exchanger is the same as the heat Q_{cond} conducted through the material.

An example of the measurement required for the evaluation of the thermal conductivity of the porous material is given in Fig. 4 for the 400 CPSI ceramic material. The two heat powers Q_{load} and Q_{amb} are plotted vs the temperature ΔT measured across the porous material. As expected, Q_{amb} increases linearly with the temperature difference ΔT, and the slope of the curve gives access to the value of the thermal conductivity of the porous material. For the 400 CPSI Celcor ceramic, the measured thermal conductivity is $k_s = 2.5$ W·m^{-1}·K^{-1}, in agreement with the value specified by the manufacturer (Corning Environmental Products Division, Corning, NY).

Figure 4 also shows the heat losses in the system represented by the difference between the heat extracted Q_{amb} and the heat injected Q_{load}. This difference is mainly due to lateral losses through the wall of the measurement vein but also to radiation on the other side of the heat exchangers. In the Appendix, the curves Q_{load} and Q_{amb} vs the temperature difference are given for all materials studied.

TABLE I. Properties of the different materials characterized ($\delta_\kappa = 266\ \mu$m at 100 Hz).

Material (supplier and catalog no.)	L (mm)	r_0 (r_0/δ_k) (μm) ([1])	ϕ (%)	k_s (W·m^{-1}·K^{-1})	$\lvert Z/Z_c\rvert_{opt}$ (1)	$(\varphi_{p/U})_{opt}$ (deg)
400 CPSI ceramic (Celcor Corning[a])	40	585 (2.20)	85.0	2.50	2.71	59.8
800 CPSI ceramic (Flora Corning[a])	40	411 (1.55)	80.0	2.61	3.76	29.0
NiCr Foam (Recemat[b] NC-1723.10)	20	494 (1.86)	76.8	2.42	2.61	40.2
Copper Foam (Recemat[b] Cu4753.05)	10	182 (0.68)	87.0	4.23	1.18	−2.5
RVC Foam (Goodfellow[c] VC003830)	12.7	173 (0.65)	82.0	0.14	8.06	−0.9
Rigid glass wool	20	74 (0.28)	87.3	1.86	5.41	−5.9
304L mesh grid (Gantois[d] 105864)	7.5	45 (0.17)	80.0	0.28	4.97	6.5

[a]Corning Environmental Products Division (Corning, NY).
[b]Recemat BV, Dodewaard, Netherlands.
[c]Supplied by Goodfellow SARL, Lille, France.
[d]Gantois Industries, Saint-Dié-des-Vosges, France.

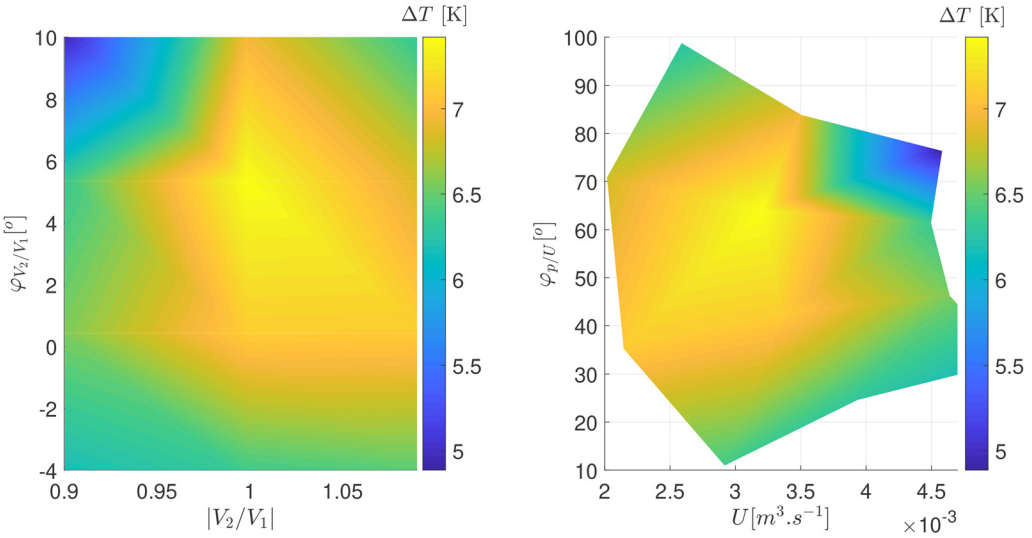

FIG. 5. (Color online) Temperature difference ΔT measured across the 400 CPSI ceramic material as a function of the amplitude ratio and phase between the two loudspeaker voltages (a) and as a function of the volume flow amplitude U and the phase between acoustic pressure and the volume flow $\varphi_{p/U}$ at the center of the material (b) for a fixed acoustic pressure of 1500 Pa.

Table I summarizes the value of k_s measured for all materials studied. The 800 CPSI Flora ceramic has a slightly higher conductivity than the 400 CPSI Celcor, as the ceramic substrates are not part of the same product range. It should also be mentioned that the three foams were chosen because the conductivities of the bulk material constituting their skeletons are quite different: close to the ceramic for NiCr foam, an order of magnitude lower for RVC foam, and higher for the copper foam.

B. Optimal acoustic field determination

An optimal acoustic field exists that maximizes the temperature difference across the material.[18] This optimal acoustic field depends on the frequency but also on the geometrical and thermo-physical characteristics of the material. The expression (11) of the optimal acoustic field being based on simplified assumptions, in the following, we will determine experimentally this acoustic field for each material studied at the fixed frequency of 100 Hz. The determination of the optimal acoustic field consists in measuring the temperature difference ΔT without heat exchangers at a fixed acoustic pressure vs two control parameters: the ratio of amplitudes $|V_2/V_1|$ and the phase shift φ_{V_2/V_1} between the voltages driving the two sources. The pressure amplitudes given by the four microphones are also measured to access the amplitude of the complex volume flow velocity $\{U, \varphi_{p/U}\}$ at the center of the material for each couple $\{|V_2/V_1|, \varphi_{V_2/V_1}\}$. A mapping is thus realized, linking the space of the control parameters—the signals driving the sources—$\{|V_2/V_1|, \varphi_{V_2/V_1}\}$ to the space of parameters of interest—the acoustic field—$\{U, \varphi_{p/U}\}$.

Figure 5 presents an example of the two mappings measured for the 400 CPSI ceramic at a fixed acoustic pressure of 1500 Pa. A preliminary measurement scans a wider range of couples $\{|V_2/V_1|, \varphi_{V_2/V_1}\}$ than the one presented here and allows us to focus, as a second step, on the measurement around the optimum value to have a more accurate evaluation of the optimum acoustic field. In the example presented here, a maximum temperature difference of 7.4 K is reached for $|V_2/V_1| = 1$ and $\varphi_{V_2/V_1} = 5.3°$, which corresponds to an optimal acoustic field in the center of the material characterized by $U_{\text{opt}} = 3.2 \times 10^{-3}$ m^3·s^{-1} and $(\varphi_{p/U})_{\text{opt}} = 63.9°$. The optimal values for $\{U, \varphi_{p/U}\}$ are measured with the same protocol for an acoustic pressure p varying from 500 to 2000 Pa by steps of 500 Pa, and the values are linearly interpolated for intermediate pressures. Figure 6 presents the

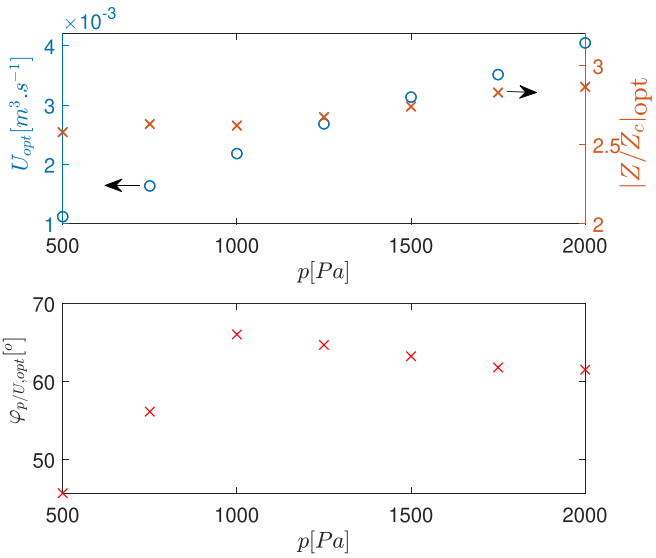

FIG. 6. (Color online) Evolution of the amplitude of the volume flow velocity and of the impedance Z at the center of the material normalized by the characteristic impedance Z_c (a) and of the phase φ_p/U (b) maximizing the temperature difference ΔT across the 400 CPSI ceramic material with the acoustic pressure p.

https://doi.org/10.1121/10.0015051

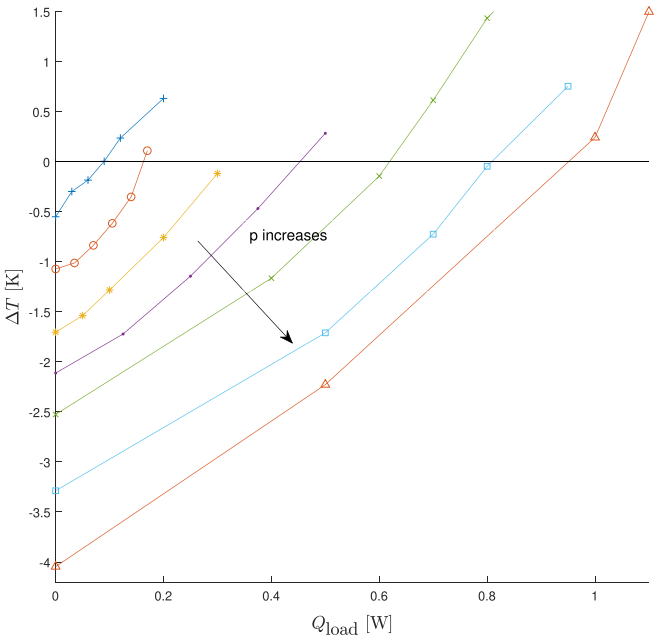

FIG. 7. (Color online) Temperature difference ΔT measured across the 400 CPSI ceramic material as a function of the thermal load Q_{load} injected for different acoustic pressures from 500 to 2000 Pa (with an increment of 250 Pa).

optimal values of $\{U, \varphi_{p/U}\}$ as a function of the acoustic pressure p. It can be observed that the acoustic volume flow U_{opt} increases linearly with the acoustic pressure. As explained in Sec. II, the linear theory predicts that U_{opt} has a fixed optimum value in the simplified case where the temperature difference across the stack is only the result of thermoacoustic heat flux and conduction within the material. It appears here that in our test-bench, the heat balance for obtaining the temperature difference is not so simple, and as observed in Fig. 4, there are non-negligible heat losses occurring to which can be added complex flow and thermal field[21] at the extremities of the porous material, which together can explain this behavior. Regarding the evolution of the optimal value of U with the acoustic pressure p, it appears relevant to consider the impedance Z at the center of the material as a function of the acoustic pressure, as given in Fig. 6. The impedance Z, normalized by the characteristic impedance Z_c of the measurement vein, and the optimal value of $\varphi_{p/U}$ remain almost constant with the acoustic pressure. Their mean values are, respectively, 2.71 and 59.8°, for the 400 CPSI ceramic.

The procedure to measure the optimal values of $|Z/Z_c|_{\text{opt}}$ and $(\varphi_{p/U})_{\text{opt}}$, which maximize the temperature difference ΔT, is repeated for all materials considered. In the Appendix (see Fig. 12), the temperature difference ΔT measured vs $|Z/Z_c|$ and $(\varphi_{p/U})$ are plotted for all materials at 1500 Pa. The mean values of $|Z/Z_c|_{\text{opt}}$ and $(\varphi_{p/U})_{\text{opt}}$ are represented [Fig. 12(g)] and are also reported in Table I for each material. The selection of materials can be classified according to their effective radius r_0 normalized by the thermal boundary layer thickness δ_κ. As expected, materials with $r_0/\delta_\kappa < 1$ behave like a regenerator with a phase $(\varphi_{p/U})_{\text{opt}}$ close to 0: the thermal cycle followed by the particle in the porous material associated with the thermoacoustic process is similar to a Stirling cycle. For material with $r_0/\delta_\kappa > 1$, the phase $(\varphi_{p/U})_{\text{opt}}$ varies from 29° (for $r_0/\delta_\kappa = 1.55$) to 60° (for $r_0/\delta_\kappa = 2.20$). The thermal cycle deviates from the Stirling cycle and gets closer to a quasi-adiabatic cycle, the optimal thickness for a quasi-adiabatic stack being $r_0/\delta_\kappa \approx 3$ [as has been demonstrated in Ref. 19 (see Fig. 5)]. The interpretation of the optimal values of $|Z/Z_c|$ is more complex since for materials with almost the same normalized effective radius, the values of the optimal normalized impedance can be quite different, e.g., the copper foam and the RVC both have $r_0/\delta_\kappa \approx 0.6$ but $|Z/Z_c|_{\text{opt}}$, respectively, of 1.18 and 8.06. This difference can be explained by the fact that the amplitude of the optimal impedance depends not only on geometrical parameters of the material but also on their thermal properties: as shown in the simplified case described by relation (11), the amplitude of the optimal impedance increases with the thermal conductivity k_s.

C. Thermoacoustic heat flux measurement

Figure 7 presents the temperature difference ΔT at the extremities of the 400 CPSI ceramic material measured vs the thermal load Q_{load} injected for different acoustic pressures when the optimal acoustic field $|Z/Z_c|_{\text{opt}}$ and $(\varphi_{p/U})_{\text{opt}}$ are imposed. As expected, the temperature difference ΔT decreases with the increasing thermal load Q_{load}. The evolution of ΔT as a function of Q_{load} appears linear for some acoustic pressures (for example, at 500 and 1000 Pa) and quadratic for others. That is why, to estimate the thermal load Q_{load} that cancels ΔT for each acoustic pressure considered, the experimental data are fitted with a linear and a quadratic regression. The regression with the minimal residual term is conserved. The x-intercepts give the thermoacoustic heat flux without temperature gradient $Q_{\text{th}}(\Delta T = 0) = Q_{\text{A}}$ for each acoustic pressure considered. The maximum temperature difference ΔT_{max} measured when there is no heat load imposed is given by the ordinate at the origin. An estimation of the thermoacoustic heat flux at this temperature difference ΔT_{max} can be performed considering that it is equivalent to the thermal power $Q_{\text{load,NoAc}}$ imposed to reach ΔT_{max} without acoustic oscillation, as illustrated in Fig. 3(d).

The evolution with the acoustic pressure of the thermoacoustic heat flux without temperature difference, with a maximum temperature difference, and with the normalized temperature difference is plotted in Fig. 8. Comparison with results of the standard linear theory described by (3) is also presented. The difference between Q_{A} and $Q_{\text{th}}(\Delta T_{\text{max}})$ is due to the presence of the acoustically induced thermal conductivity flux Q_{D}, which decreases the heat flux with temperature difference. In this same figure are also represented the results for the 800 CPSI ceramic material. For the 400 CPSI ceramic, there is a good agreement between experimental and theoretical data, meaning that the linear theory is

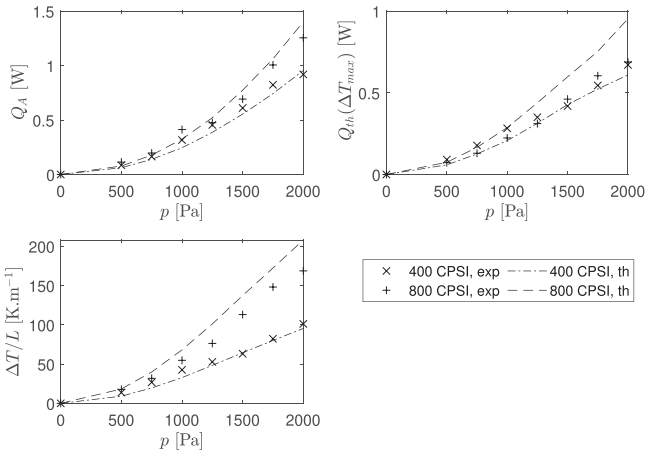

FIG. 8. Comparison among the thermoacoustic heat flux Q_A (a), $Q_{th}(\Delta T_{max})$ (when $Q_{load} = 0$) (b), and the temperature difference ΔT normalized by the material length L (c) measured (symbols) and predicted (line) vs the acoustic pressure p for the 400 and 800 CPSI ceramic materials.

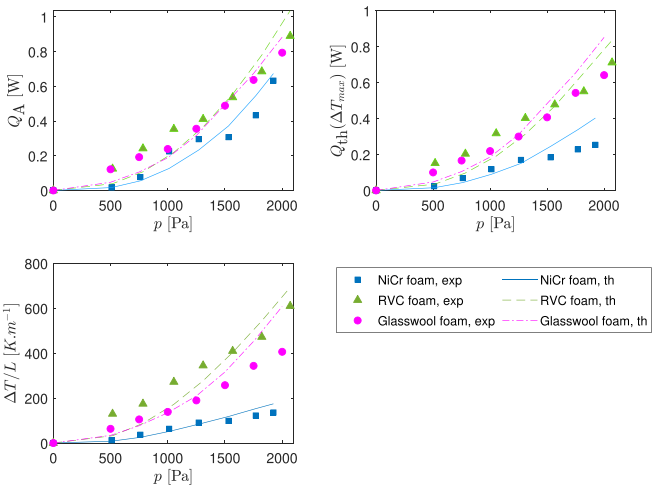

FIG. 10. (Color online) Comparison among the thermoacoustic heat flux Q_A (a), $Q_{th}(\Delta T_{max})$ (when $Q_{load} = 0$) (b), and the temperature difference ΔT normalized by the material length L (c) measured (symbols) and predicted by Swift formulation (line) vs the acoustic pressure p for different materials.

suitable for describing this ceramic, at least up to drive ratios of 2%. This good agreement also allows us to validate the measurement method. Small deviation appears beyond a drive ratio of 1% for the 800 CPSI ceramic, and the model becomes insufficient due to poorly described phenomena, such as aerodynamical and thermal edge effects in the vicinity of the stack ends and heat exchangers,[21,22] or perhaps due to a temperature distribution that might not remain one-dimensional.

Figures 9(a)–9(c) show the experimental thermoacoustic heat flux Q_A, $Q_{th}(\Delta T_{max})$ and the temperature difference ΔT normalized by the material length measured vs the acoustic pressure for the stacked-screen material and also for the copper foam. For comparison, the theoretical thermoacoustic heat flux calculated from the linear theory (3) and from empirical equation (8) of Swift and Ward are shown, respectively, by dashed lines and solid lines. There is a good agreement between the theoretical and experimental heat flux for the stacked-screen. The differences between the two proposed models are minor. In fact, the measurements are performed for this material at a normalized impedance of $|Z/Z_c|_{opt}$ of about 4.97, which leads to a maximum velocity value inside the material of about 1.2 m·s^{-1} at 2000 Pa. The Swift formulation initially developed for mesh screen material is also implemented here for the copper foam. The measurements for copper foam are carried out at a normalized impedance of 1.18, which leads to a maximum velocity of 3.5 m·s^{-1} inside the material at 2000 Pa, which is more important than the velocity inside

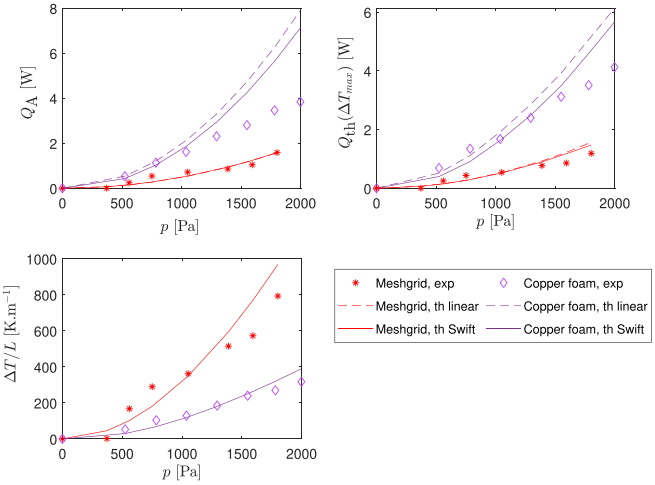

FIG. 9. (Color online) Comparison among the thermoacoustic heat flux Q_A (a), $Q_{th}(\Delta T_{max})$ (when $Q_{load} = 0$) (b), and the temperature difference ΔT normalized by the material length L (c) measured (symbols) and predicted by the linear theory (dashed line) and by the Swift and Ward model (line) vs the acoustic pressure p for the copper foam and the mesh screen.

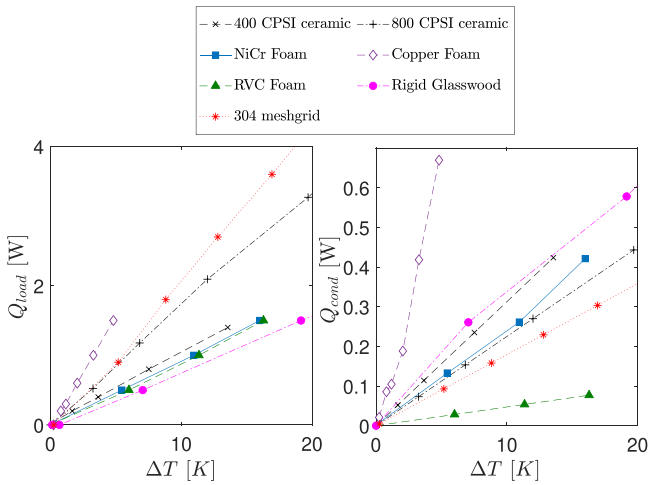

FIG. 11. (Color online) Thermal load (without acoustic wave) Q_{load} and heat conduction Q_{cond} measured vs the temperature difference ΔT for all investigated materials.

https://doi.org/10.1121/10.0015051

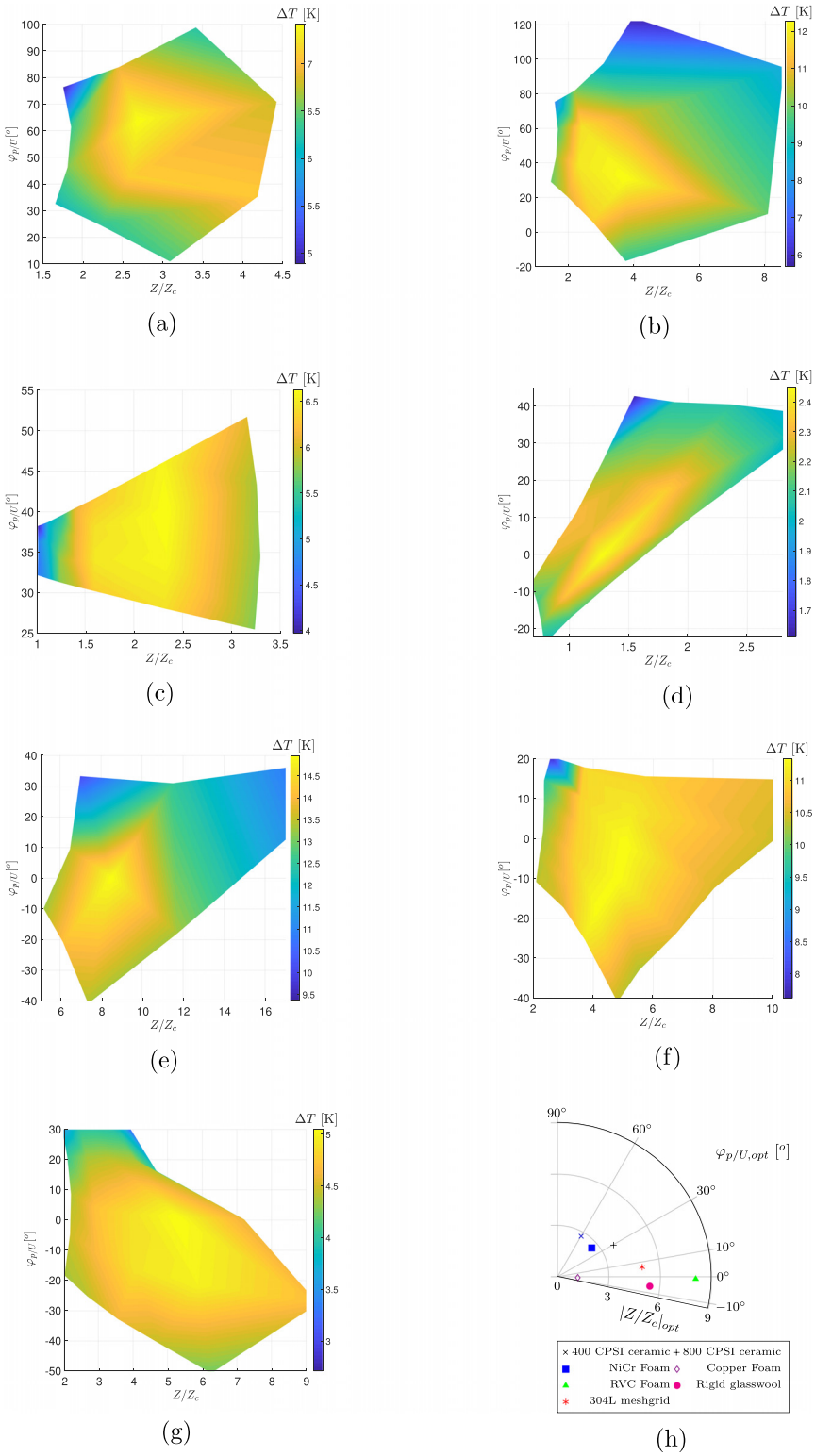

FIG. 12. (Color online) (a)–(f) Temperature difference ΔT as a function of the amplitude of impedance Z normalized by the characteristic impedance and the phase between acoustic pressure and the volume flow $\varphi_{p/U}$ at the center of the material, for a fixed acoustic pressure of 1500 Pa and for all studied materials. (g) Representation of the mean optimal values of $|Z/Z_c|_{\text{opt}}$ and $(\varphi_{p/U})_{\text{opt}}$ for all studied materials.

the mesh screen. For this reason, the results of the two models are no longer superimposed for this material. It should be noted that the acoustic Reynolds number Re_{ac} defined by $v_x\delta_\nu/\nu$ (Ref. 23) at 100 Hz for the maximum velocity value measured (which is 3.5 m·s^{-1} found in the copper foam) is 51, meaning that the acoustic flow remains laminar for the copper foam and by extension for all the materials under test. The agreement between the experimental results and the two models is not as good as that obtained for ceramic materials but remains quite acceptable. As the theoretical curve obtained via the Swift model is closer to the experimental one and seems to describe more precisely the heat flux, this model is retained for the study of other materials.

As mentioned previously for the 800 CPSI ceramic, the model becomes insufficient as it does not take into account the aerodynamical and thermal edge effects in the thermoacoustic core,[21,22,24] and it assumes that the temperature distribution remains one-dimensional. This deviation from simple theory was also observed by Poese and Garrett[25] in an operational stack-based thermoacoustic refrigerator at drive ratios $\geq 3\%$. Figures 10(a)–10(c) show the relation between the experimental and theoretical heat flux vs the acoustic pressure for the NiCr foam, RVC foam, and glass wool materials. As expected, the thermoacoustic heat flux Q_A and $Q_{th}(\Delta T_{max})$ rise quadratically with the acoustic pressure p. It should be noted that these materials have different characteristics in terms of effective radius with respect to the thermal boundary layer that classifies them as regenerators (for the RVC foam and glass wool) or as stack (for the NiCr foam) or in terms of heat conductivity (from $k_s = 0.14$ W·m^{-1}·K^{-1} for the RVC foam to 2.42 W·m^{-1}·K^{-1} for the NiCr foam). Despite these differences, the agreement between theoretical and measured values is sufficient to prove that the measurement method presented in this paper remains valid on a wide range of materials. However, a refinement of the theoretical model seems necessary to account for both the specificity of the porous materials and complex phenomena that are not captured satisfactorily (such as stack ends effect or non-one-dimensional temperature field).

V. CONCLUSION

In this paper, an experimental test-bench has been specially developed to characterize various materials in air at atmospheric pressure for refrigeration purposes. This test-bench enables, on the one hand, identification of the optimal acoustic field that maximizes the temperature difference at the ends of the material at different acoustic amplitudes and, on the other hand, access to the thermoacoustic heat transport through the materials via a protocol specifically implemented. Measurements on straight-pore materials allow us to validate the experimental results by comparison with an analytic model available for this geometry. Then more complex materials used in classical high power machines were investigated, and the comparison with theoretical results shows a reasonable agreement. The protocol implemented here with air at atmospheric pressure can be transposed to another fluid (e.g., a pressurized inert gas as commonly employed in thermoacoustic refrigerators) to be similar to the conditions of a real machine. Such a transposition can be accomplished using the techniques discussed by Olson and Swift.[26] Results from this experimental campaign, obtained at a single frequency and for only one length of the material, open perspectives in choosing appropriate stack material and geometry for actual machines relying on the thermoacoustic effect, given the constraints of the geometry, the working fluid, etc.

ACKNOWLEDGMENTS

This work has been supported by the French National Agency for Research (Project No. TACOT ANR-17-CE06-0007). The authors would like to thank a student, Fabrizio Salvati, who has worked on this project during his master's internship.

APPENDIX

In Sec. IV A, the results for the thermal measurements without acoustic oscillation are presented for the 400 CPSI ceramic material. Here, we present the corresponding experimental results for all materials. Figure 11 represents the heat fluxes Q_{load} and $Q_{amb} = Q_{cond}$ vs the temperature difference $\Delta T_{No,Ac}$. From these curves, we can deduce the thermal conductivity k_s (given in Table I) as well as the thermal losses Q_{loss} at a given temperature difference required to measure the heat flux $Q_{th}(\Delta T_{max})$.

In addition, Fig. 12 presents the mapping of the temperature difference measured vs the parameters $\{U, \varphi_{p/U}\}$ for each material at a fixed acoustic pressure of 1500 Pa. These maps highlight that the values of optimal acoustic field vary from one material to another.

[1]G. W. Swift, *Thermoacoustics: A Unifying Perspective for Some Engines and Refrigerators*, 2nd ed. (Springer, Cham, Switzerland, 2017).
[2]F. W. Giacobbe, "Estimation of Prandtl numbers in binary mixtures of helium and other noble gases," J. Acoust. Soc. Am. **96**(6), 3568–3580 (1994).
[3]P. Merkli and H. Thomann, "Thermoacoustic effects in a resonance tube," J. Fluid Mech. **70**(1), 161–177 (1975).
[4]T. Jin, H. Jiale, Y. Feng, R. Yang, K. Tang, and R. Radebaugh, "Thermoacoustic prime movers and refrigerators: Thermally powered engines without moving components," Energy **93**, 828–853 (2015).
[5]M. E. Poese, R. W. M. Smith, S. L. Garrett, R. van Gerwen, and P. Gosselin, "Thermoacoustic refrigeration for ice cream sales," in *Proceedings of the 6th IIR-Gustav Lorentzen Natural Working Fluids Conference*, Glasgow, UK (August 29–September 1, 2004).
[6]M. Tijani and S. Spoelstra, "Study of a coaxial thermoacoustic-Stirling cooler," Cryogenics **48**(1), 77–82 (2008).
[7]G. Poignand, A. Podkovskiy, G. Penelet, P. Lotton, and M. Bruneau, "Analysis of a coaxial, compact thermoacoustic heat-pump," Acta Acust. united Acust. **99**(6), 898–904 (2013).
[8]I. A. Ramadan, H. Bailliet, G. Poignand, and D. L. Gardner, "Design, manufacturing and testing of a compact thermoacoustic refrigerator," Appl. Therm. Eng. **189**, 116705 (2021).
[9]J. Xu, J. Hu, E. Luo, J. Hu, L. Zhang, and S. Hochgreb, "Numerical study on a heat-driven piston-coupled multi-stage thermoacoustic-stirling cooler," Appl. Energy **305**, 117904 (2022).
[10]N. Rott, "Thermally driven acoustic oscillations, part III: Second-order heat flux," Z. Angew. Math. Phys. **26**(1), 43–49 (1975).
[11]G. W. Swift and W. C. Ward, "Simple harmonic analysis of regenerators," J. Thermophys. Heat Trans. **10**(4), 652–662 (1996).
[12]Y. Ueda, T. Kato, and C. Kato, "Experimental evaluation of the acoustic properties of stacked-screen regenerators," J. Acoust. Soc. Am. **125**(2), 780–786 (2009).
[13]S. H. Hsu and T. Biwa, "Modeling of a stacked-screen regenerator in an oscillatory flow," Jpn. J. Appl. Phys. **56**(1), 017301 (2017).
[14]H. S. Hsu and T. Biwa, "Measurement of heat flow transmitted through a stacked-screen regenerator of thermoacoustic engine," Appl. Sci. **7**(3), 303 (2017).
[15]A. S. Abduljalil, Z. Yu, and A. J. Jaworski, "Selection and experimental evaluation of low-cost porous materials for regenerator applications in thermoacoustic engines," Mater. Des. **32**(1), 217–228 (2011).
[16]G. W. Swift and R. M. Keolian, "Thermoacoustics in pin-array stacks," J. Acoust. Soc. Am. **94**, 941–943 (1993).

[17]W. M. Kays and A. L. London, *Compact Heat Exchangers*, 3rd ed. (McGraw-Hill, New York, 1984).
[18]G. Poignand, B. Lihoreau, P. Lotton, E. Gaviot, M. Bruneau, and V. Gusev, "Optimal acoustic fields in compact thermoacoustic refrigerators," Appl. Acoust. **68**(6), 642–659 (2007).
[19]G. Poignand, P. Lotton, G. Penelet, and M. Bruneau, "Thermoacoustic, small cavity excitation to achieve optimal performance," Acta Acust. united Acust. **97**(6), 926–932 (2011).
[20]M. Munjal and A. Doige, "Theory of a two source-location method for direct experimental evaluation of the four-pole parameters of an aero-acoustic element," J. Sound Vib. **141**(2), 323–333 (1990).
[21]A. Berson and P. Blanc-Benon, "Nonperiodicity of the flow within the gap of a thermoacoustic couple at high amplitudes (L)," J. Acoust. Soc. Am. **122**(4), EL122–EL127 (2007).
[22]P. Blanc-Benon, E. Besnoin, and O. Knio, "Experimental and computational visualization of the flow field in a thermoacoustic stack," C. R. Méc. **331**(1), 17–24 (2003).
[23]P. Merkli and H. Thomann, "Transition to turbulence in oscillating pipe flow," J. Fluid Mech. **68**(3), 567–576 (1975).
[24]I. A. Ramadan, H. Bailliet, and J.-C. Valière, "Experimental investigation of oscillating flow characteristics at the exit of a stacked mesh grid regenerator," J. Acoust. Soc. Am. **149**(2), 807–818 (2021).
[25]M. E. Poese and S. L. Garrett, "Performance measurements on a thermoacoustic refrigerator driven at high amplitudes," J. Acoust. Soc. Am. **107**(5), 2480–2486 (2000).
[26]J. R. Olson and G. W. Swift, "Similitude in thermoacoustics," J. Acoust. Soc. Am. **95**(3), 1405–1412 (1994).